



# Magnesium bromide/aniline magnesium bromide sustained-release layer enables highly efficient Mg metal anode

Yichao Zhuang, Haiming Hua, Yaoqi Xu, Fei Wang, Jiayue Wu, Jing Zeng<sup>\*</sup>, Jinbao Zhao<sup>\*</sup> 

College of Chemistry and Chemical Engineering, State-Province Joint Engineering Laboratory of Power Source Technology for New Energy Vehicle, State Key Laboratory of Physical Chemistry of Solid Surfaces, Engineering Research Center of Electrochemical Technology, Ministry of Education, Collaborative Innovation Center of Chemistry for Energy Materials, Xiamen University, Xiamen 361005 China

## ARTICLE INFO

### Keywords:

Rechargeable magnesium batteries  
Mg metal anode  
Sustained-release layer  
Mg<sup>2+</sup> solvation optimization  
Anode/electrolyte interphase

## ABSTRACT

The application of conventional electrolytes in rechargeable magnesium batteries is obstructed by their incompatibility with Mg metal anode. Herein, a functional layer with sustained-release effect is constructed on Mg metal by chemical reaction between p-bromoaniline and Mg to realize compatibility between conventional electrolyte and Mg anode in the long cycle. It is proved that the functional layer contains a large amount of MgBr<sub>2</sub>, aniline magnesium bromide and their derivatives, which are released into the electrolyte. The experiment and theoretical calculation certified that the dissolved MgBr<sub>2</sub> alters the Mg<sup>2+</sup> solvation structure distribution and accelerates the desolvation process dramatically. Compared to adding additives to the electrolyte directly, the residual sustained-release layer maintains the freshness of SEI and is more conducive to the formation of Br<sup>-</sup> coordinated Mg<sup>2+</sup>. As a result, Mg electrodes with this functional layer maintains a low polarization voltage of 0.2–0.4 V at a high current density of 1.0 mA cm<sup>-2</sup> above 1000 h without short circuit. The Mg||Mo<sub>6</sub>S<sub>8</sub> battery presents a low overpotential of ~ 0.25 V during discharge/charge and remains 68.6 mAh/g after 300 cycles at the current density of 25 mA g<sup>-1</sup>, confirming the practicability of this strategy.

## 1. Introduction

As a mature energy storage technology, lithium-ion batteries (LIB) have been extensively used in mobile devices and electrical vehicles [1–3]. But the high cost, rarity and uneven distribution of lithium resources and potential safety hazards limit further development and application of LIB. In a variety of post lithium-ion batteries, rechargeable magnesium batteries (RMB) have the advantages of low cost, high energy density, safety and reliability, which make up for the shortage of LIB [4–7]. Similar to Li metal, due to high reactivity, Mg metal tends to react with the conventional ester or ether-based electrolyte to generate the solid electrolyte interphase (SEI). However, as illustrated in Fig. 1a, the intrinsic bivalency of Mg<sup>2+</sup> brings it a high charge density and strong Coulombic interaction, resulting in its inability to conduct in solid phase [8,9]. Simultaneously, strong Coulombic interaction between Mg<sup>2+</sup> and solvation structure also enhances the activation energy of Mg<sup>2+</sup> desolvation process, exacerbating the decomposition of electrolytes at high current density [10–12]. Consequently, Mg metal anode is severely passivated in conventional electrolytes, exhibiting extremely high overpotential (> 2 V) and irreversible stripping/plating behavior

(Coulombic efficiency < 60 %) [13,14]. The efficient usage of the Mg metal is the premise to ensure the advantages of RMB, and considerable effort has been expended on Mg metal anode/electrolyte interphase.

In the earlier study, the solution for the problems above focused on stabilizing the Mg anode, so that the Mg does not react with the electrolyte to avoid the formation of passivation film and achieve highly reversible stripping/plating behavior, such as the development of Grignard-based, organoborate-based electrolytes system [15–17]. Nevertheless, these electrolytes still have limitations. For example, Grignard-based electrolyte have the flaws of low anodic stability, Cl<sup>-</sup> corrosion and strong Mg-Cl bond [18,19], and the organoborate-based electrolyte has the problems of expensive raw materials, complicated preparation process and high cost [20,21]. In contrast, the conventional Mg electrolytes, such as Mg(PF<sub>6</sub>)<sub>2</sub> or magnesium bis(trifluoromethanesulfonyl)imide (Mg(TFSI)<sub>2</sub>) etc. dissolved in ether, ester or nitrile solvents not only avoid complicated preparation processes, but also have higher anodic stability to match cathodes with higher voltages [22–24]. The difficulty in the application of conventional Mg electrolytes lies in the passivation of Mg caused by uncontrolled decomposition of anions and solvent [25–28]. The compatibility between conventional

<sup>\*</sup> Corresponding authors.

E-mail addresses: [zengjing@xmu.edu.cn](mailto:zengjing@xmu.edu.cn) (J. Zeng), [jbzha@xmu.edu.cn](mailto:jbzha@xmu.edu.cn) (J. Zhao).

<https://doi.org/10.1016/j.cej.2025.159445>

Received 26 August 2024; Received in revised form 6 January 2025; Accepted 8 January 2025

Available online 9 January 2025

1385-8947/© 2025 Elsevier B.V. All rights are reserved, including those for text and data mining, AI training, and similar technologies.

electrolyte and Mg anode can be realized by constructing functional layer on Mg surface to prevent Mg metal passivation and electrolyte decomposition. Since Ban et al. initially constructed an artificial interphase on Mg powder to enable the reversible Mg plating/stripping in ester-based electrolyte [29], several novel functional layers have been tailored in recent years to realize compatibility between conventional electrolyte and Mg metal anode [30–35]. Among these works, metal (M)/MgX<sub>2</sub> (M=Sn, Bi, Zn, Si, etc., X=Cl, F, Br, I, etc.) layer made by ion-exchange and alloying reactions of Mg metal with MX<sub>2</sub>/ether is a prospective way to reduce Mg stripping/plating overpotential [36–44]. Our group have also proposed a simple and effective Bi@PTHF hybrid layer strategy to achieve high efficiency Mg anode with a low polarization voltage of ~ 0.25 V in Mg(TFSI)<sub>2</sub>/DME electrolyte [45]. Besides, halogenated organics has a similar reaction that can generate magnesium halide on the Mg metal. Lee et al. chemically activated the Mg metal by the reaction between dibromoethane and Mg to reduce the polarization voltage of Mg symmetric cell to less than 0.5 V and increase the lifespan to over 150 h (1.0 mA cm<sup>-2</sup>) [46]. At present, the functional layer made by this approach are believed to be relatively stable in the electrolyte, which plays the role of Mg<sup>2+</sup> ionic conductor and isolates parasitic reactions. However, although MgX<sub>2</sub> is difficult to dissolve directly in ether solvents, it can form complex and then dissolve in the electrolyte containing Mg<sup>2+</sup>. Thus, the dissolution of SEI is often overlooked, thus masking the true mechanism of this SEI.

Because aniline molecules can be adsorbed on the surface of Mg and have the potential effect of regulating the solvation structure of Mg<sup>2+</sup>, functional layers formed by halogenates of aniline may have better electrochemical performance. Compared with bromine aniline, the chloride aniline cannot react with Mg metal since its Cl atom is difficult to leave. Based on the spatial effect, in this study, p-bromoaniline (p-BAn) is used to react with Mg metal and constructs a sustained-release layer composed of aniline magnesium bromide and magnesium bromide and their derivatives on the surface. As exhibited in Fig. 1b, aniline magnesium bromide and magnesium bromide species contained in the sustained-release layer are released into the electrolyte until saturation, which alters the solvation structure distribution in the electrolyte and eliminates contaminants such as trace H<sub>2</sub>O in the electrolyte. Additionally, the residual functional layer on the Mg metal can maintain the activity of SEI. As a consequence, the intrinsically inefficient Mg metal anode promotes electrochemical performance and possesses highly

reversible Mg stripping/plating characteristics. At the current density of 1.0 mA cm<sup>-2</sup>, the polarization voltage of Mg symmetrical cell is reduced from ~ 2 V to < 0.4 V, and the cycling life is extended from 50 h to 1000 h.

## 2. Result and discussion

### 2.1. Formation of functional layer

As bromide of aniline, p-BAn have similar adsorption on Mg surface and potential ability of inducing pseudo-Grignard reagent species [47,48]. As shown in Fig. S1, Mg metal reacts with a high concentration of p-BAn/DME solution to form a black functional layer on its surface. The speculated mechanism of the reaction between Mg and p-BAn is shown in Fig. S2. Eventually, the final solution is a mixture of PhNHMgBr, (PhNH)<sub>2</sub>Mg, MgBr<sub>2</sub>, etc [46] and the functional layer is formed from the precipitation of product above. In order to verify the product of the reaction between Mg and p-BAn/DME solution, <sup>1</sup>H nuclear magnetic resonance (NMR) spectra of the solution before and after the reaction were measured (Fig. 2a). The a and b peaks represent the *meso*-site and *ortho*-site H atoms of the benzene ring, while c represents the H atoms of -NH<sub>2</sub>. After the reaction, a and c shift to the lower field while b moves to the higher field, which is consistent with the transition trend of p-bromoaniline to aniline (Fig. S3).

After the activation of Mg, the morphology of functional layer can be seen in Fig. 2b and S4. The functional layer on the Mg metal is even and intact, and the thickness of functional layer is about 10 μm. Energy dispersive spectrometer (EDS) (Table S1 and Fig. S5) indicates that the main element of the functional layer are C, O, Mg and Br, which are distributed uniformly and the ratio of Mg to Br is nearly 1:2. To identify the component of functional layer, X-ray diffraction (XRD) is carried out to characterize the surface of the modified Mg. As shown in Fig. 2c, the peaks of MgBr<sub>2</sub> and its hydrates (produced during the transfer of samples) can be found, which proves the existence of MgBr<sub>2</sub> in the functional layer. In addition, there are some unrecognized peaks with high intensity, which are assumed to be complexes of MgBr<sub>2</sub> and DME molecules according to the high content of C and O in functional layer in EDS analysis. To explore the organic components contained in the functional layer, attenuated total reflectance infrared absorption spectrometry (ATR-IR) is performed on the modified Mg electrode (Fig. 2d) and the IR

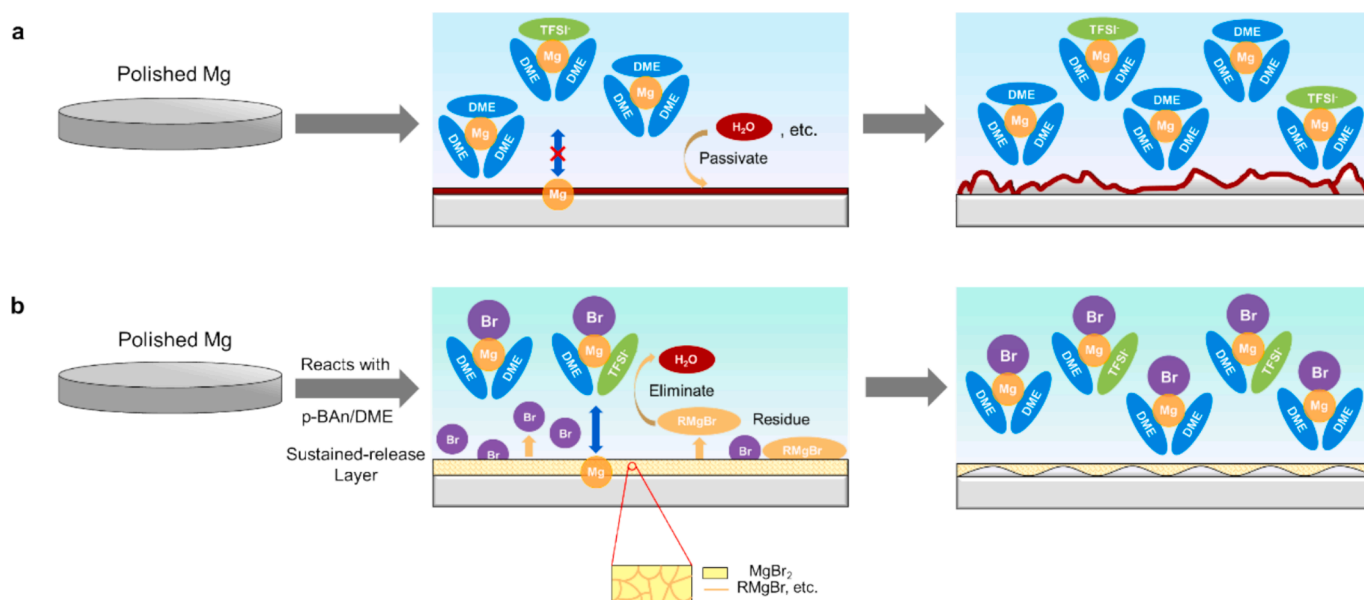


Fig. 1. Illustration of (a) the Mg stripping/plating behaviors of bare Mg in Mg(TFSI)<sub>2</sub>/DME electrolyte and (b) magnesium bromide/aniline magnesium bromide sustained-release layer promote Mg stripping/plating.

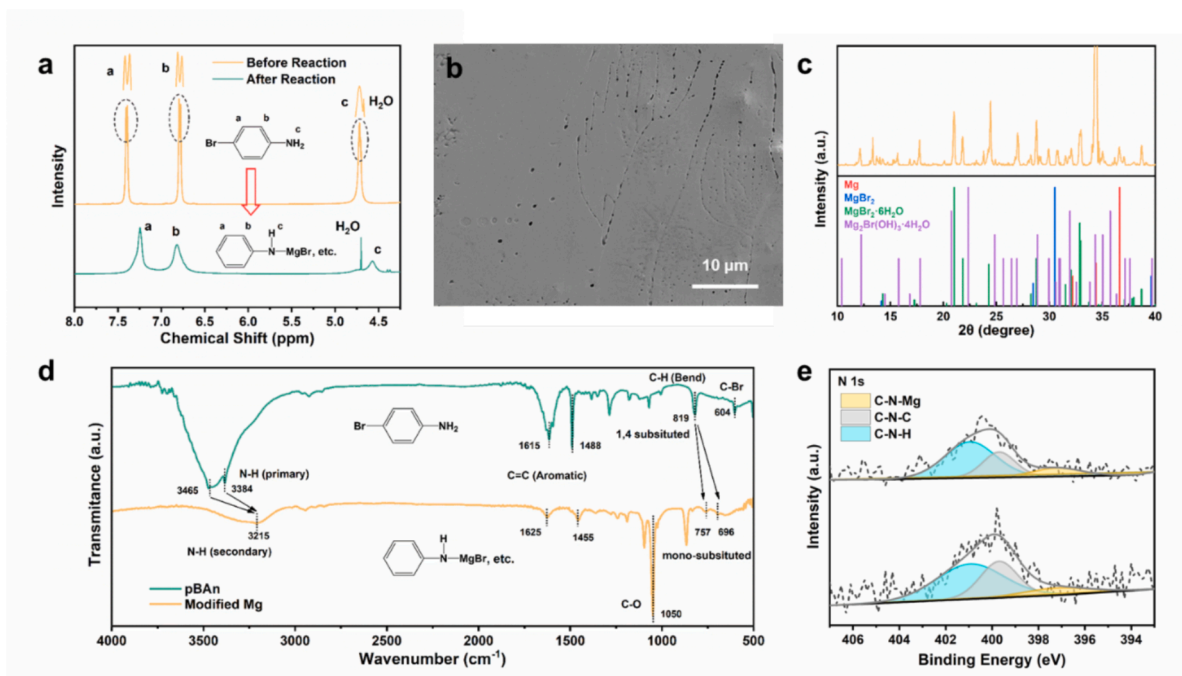


Fig. 2. (a)  $^1\text{H}$  NMR spectra of p-BAN/DME solution before and after the addition of Mg. (b) Surface SEM images of modified Mg. (c) The XRD pattern of the modified Mg. (d) IR spectra of p-BAN and modified Mg. (e) High-resolution XPS N1s spectra of the modified Mg electrodes.

spectrum of p-BAN is measured as a reference. After the reaction between p-BAN and Mg metal, the peaks of the benzene ring C-C bond represented at 1615, 1488  $\text{cm}^{-1}$  did not have obvious shift, indicating the retention of benzene ring. The disappearance of the peak that represents C-Br bond stretching vibration at 604  $\text{cm}^{-1}$  manifests it was replaced by C-H. The peak of C-H bond of 1,4 substituted benzene ring flexural vibration at 819  $\text{cm}^{-1}$  was shifted to the double peaks at 757 and 696  $\text{cm}^{-1}$ , which represented the C-H bond of single substituted benzene ring. The double peaks represented N-H stretching vibration at 3384, 3485  $\text{cm}^{-1}$  shifted to a single peak at 3215  $\text{cm}^{-1}$ , proving that the aniline is converted from primary amine to secondary amine. In addition, the intensity of the peak C-O bond at 1050  $\text{cm}^{-1}$  is enhanced, which is consistent with previous speculation about the coordination of DME molecules and  $\text{MgBr}_2$ . Based on the IR spectra analysis above, the functional layer contains the aniline magnesium bromide or its polymers, which might be intrinsically redox active. Additionally, the X-ray photoelectron spectroscopy (XPS) spectra of the modified Mg electrode are measured and shown in Fig. S6. Among these high-resolution XPS spectra (Fig. S7), the peaks in 397.2 eV (Fig. 2e) is attributed to N from C-N-Mg [49], which confirms the existence of aniline magnesium bromide. In summary, the main components of the functional layer are the aniline magnesium bromide ( $\text{PhNHMgBr}$ ) or its derivatives, magnesium bromide ( $\text{MgBr}_2$ ) and its complex with DME molecules.

## 2.2. Electrochemical characterization of modified Mg

The bare Mg and modified Mg electrodes are assembled into symmetric cells with 0.5 M  $\text{Mg}(\text{TFSI})_2/\text{DME}$  electrolyte to compare their electrochemical performance. As shown in Fig. 3a, at the current density of 1.0  $\text{mA cm}^{-2}$ , the polarization voltage of the symmetric cells with bare Mg is about 2–3 V, and the lifespan is only about 50 h, which are caused by serious passivation and uneven deposition on the surface of Mg metal. After the Mg electrodes are modified by p-BAN, the polarization voltage of the cell maintains at 0.2–0.4 V above 1000 h without short circuit. Even at the higher current density of 5  $\text{mA cm}^{-2}$  (Fig. 3b), the symmetric cell with the modified Mg still maintains a low polarization voltage of about 0.6 V.

In Cu-Mg asymmetrical cells with different Mg electrodes, as shown in Fig. 3c–e, the polarization voltage of magnesium symmetric cells without any modification is still 2–3 V, and the average Coulombic efficiency is less than 5%. The polarization voltage of the Mg-Cu cells can be reduced to < 0.2 V and the average Coulombic efficiency can be increased to about 94%. Theoretically, the modification on the Mg would not increase the Coulombic efficiency of the Cu electrode. The increase in the Coulombic efficiency of the Mg-Cu cells implies that some components in the functional layer are released in the electrolyte and optimize Mg stripping/plating process on Cu electrode.

To verify the dissolution of functional layer and its effect on the Mg stripping/plating, the modified Mg are fully immersed in the equivalent 0.5 M  $\text{Mg}(\text{TFSI})_2/\text{DME}$  electrolyte to obtain the modified electrolyte. As shown in Fig. S8a, the polarization voltage of the symmetric cell is also significantly reduced, demonstrating that the materials released into the electrolyte can enhance the stripping/plating process. The performance of Cu-Mg asymmetrical cells is also shown in Fig. 3f–g. During the first few cycles, high interfacial activity brought by the functional layer creates better electrochemical performance of the modified Mg than electrolyte modification. With the activation of electrode/electrolyte interphase, the polarization voltage and Coulombic efficiency of the modified electrolyte and modified Mg reach similarity eventually (Fig. 3g–h). The hysteresis in the improvement of Mg stripping/plating process by the modified electrolyte indicates the superiority of the modified Mg. The modified Mg electrodes soaked in electrolyte are rinsed with DME and assembled into Mg symmetrical cells as well. Although the polarization voltage of the symmetric cell is reduced to ~ 0.5 V, the cycling life of the cell is reduced to ~ 10 h (Fig. S8b), indicating that the functional layer on the Mg metal is still residual and continues to affect its electrochemical performance. In short, the electrochemical performance of the modified electrolyte and soaked Mg suggests that functional layer dissolved into the  $\text{Mg}(\text{TFSI})_2/\text{DME}$  electrolyte partially, which would affect the electrochemical property of the electrolyte dramatically.

As shown in Fig. S9a and b, when the concentration of  $\text{MgBr}_2$  in the 0.5 M  $\text{Mg}(\text{TFSI})_2/\text{DME}$  electrolyte reaches 0.5 M, it becomes supersaturated and forms colloids, which cannot dissolve any more  $\text{MgBr}_2$ . When

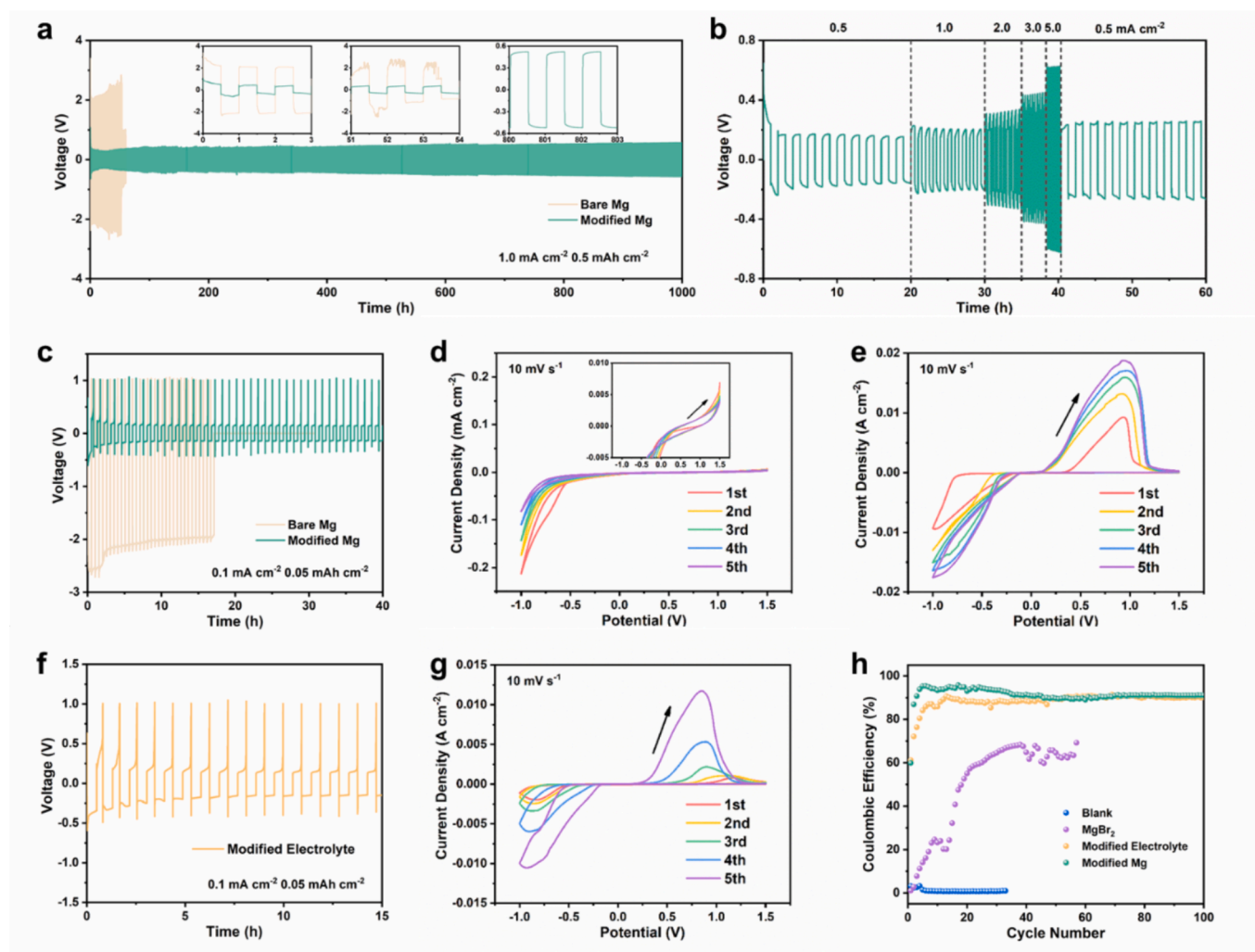


**Fig. 3.** (a) The galvanostatic voltage profiles of the bare Mg and the modified Mg symmetric cells with 0.5 M Mg(TFSI)<sub>2</sub>/DME electrolyte. (b) The voltage profiles of the modified Mg symmetric cells with various current density. (c) The galvanostatic voltage profiles of Cu-Mg asymmetrical cells with the bare Mg electrodes and the modified Mg. The cyclic voltammograms of Mg//Cu cells with the (d) bare Mg electrodes and (e) modified Mg. (f) The galvanostatic voltage profiles of Mg//Cu cells with modified Mg and modified electrolyte. (g) The cyclic voltammograms of Mg//Cu cells with the modified electrolyte. (h) The Coulombic efficiency of Cu-Mg asymmetrical cells with different electrolyte or Mg.

the concentration of MgBr<sub>2</sub> is increased to 0.6 M, Mg salt precipitates. In Fig. S9c, when 0.01 M MgBr<sub>2</sub> is added to pure DME solvent, it will precipitate rather than dissolve, which explains why MgBr<sub>2</sub> is not released during the preparation of artificial SEI. When the p-BAN modified Mg symmetric cell is assembled with pure DME solvent as the electrolyte, it could only charge/discharge at a low current density ( $\sim 0.01 \text{ mA cm}^{-2}$ ), indicating a low Mg<sup>2+</sup> concentration in DME solvent (Fig. S10).

Based on the experimental phenomena above, we chose 0.5 M Mg(TFSI)<sub>2</sub> + 0.5 M MgBr<sub>2</sub>/DME as the reference electrolyte more evidently. As shown in Fig. S11a, the polarization voltage of the Mg symmetric cells is reduced to 0.4–0.5 V (except for the first cycle), but the lifespan is still only about 10 h. For the Mg-Cu asymmetrical cells with MgBr<sub>2</sub> containing electrolyte (Fig. S11b), the polarization voltage is reduced to about 0.5 V and the average Coulombic efficiency is increased to 40 %, but the cycling life is only about 40 h. The short lifespan of Mg symmetric and Mg-Cu asymmetrical cells indicates that the plating in these electrolytes are severely uneven. It also can be inferred from the polarization voltage decrease brought by MgBr<sub>2</sub> addition that the dissolution of MgBr<sub>2</sub> from the functional layer may be one of the reasons for the improved electrochemical performance of the modified Mg. We also tried adding 2 M p-BAN directly to the electrolyte, as shown in Fig. S12a.

Although relevant literature reports that aniline adsorbed on the surface of Mg metal to reduce the overpotential of Mg, the addition of p-BAN in the electrolyte does not result in a similar improvement. The polarization voltage of the Mg symmetric cell is higher than that of the modified Mg obviously. The reaction between p-BAN and Mg might destroy the anti-passivation effect of the aniline molecules, and the further reaction of p-BAN with Mg is blocked by the contaminants in electrolyte (Fig. S12b). Eventually, neither the adsorption of p-BAN can be realized, nor the functional layer can be constructed.

### 2.3. Dissolution of functional layer

To further investigate the dissolution of functional layer and its influence on electrolyte, firstly, the soaked Mg is characterized with SEM and XRD. The SEM image exhibited in Fig. 4a indicating that the modified Mg still has a thin functional layer on the surface after soaking in the electrolyte. There is still an amount of Br on the surface of magnesium metal, which is less than that before soaking (Table S2 and Fig. S13). Nevertheless, no obvious MgBr<sub>2</sub> or its complex peaks can be found in XRD pattern of soaked Mg (Fig. 4b), implying the mass dissolution of MgBr<sub>2</sub>. The corresponding dissolved substance can also be proved from the electrolyte side. The LSV curve of different electrolytes

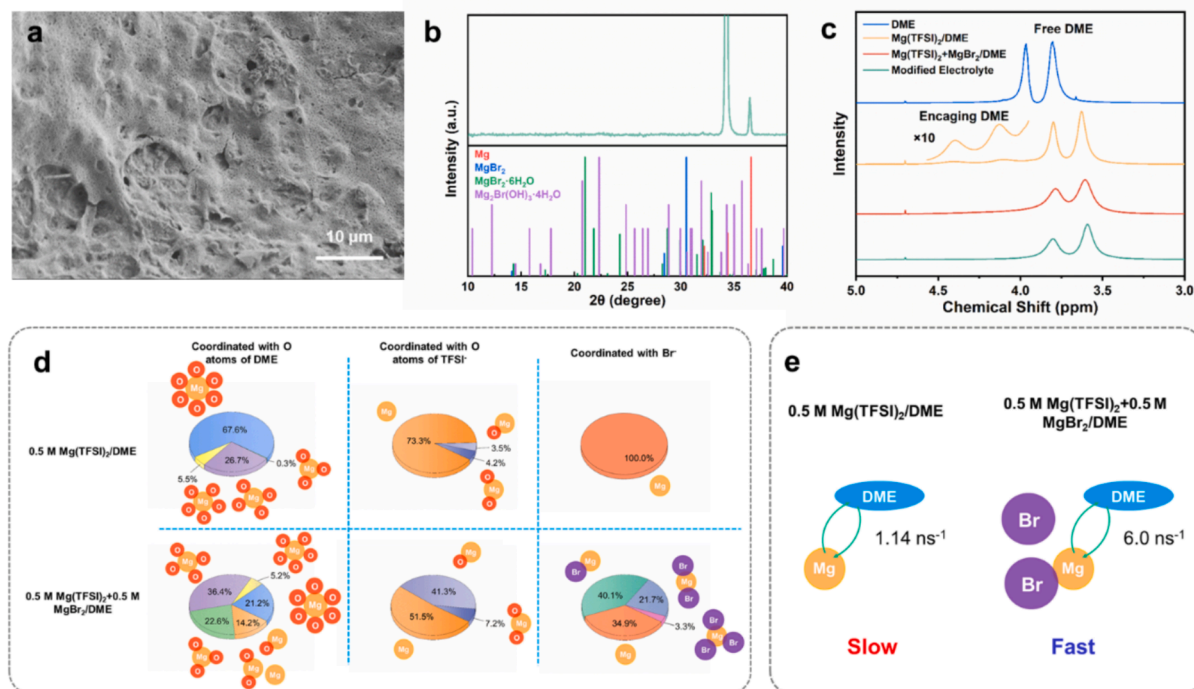


**Fig. 4.** (a) The SEM image of the soaked Mg. (b) The XRD pattern of the soaked Mg electrode. (c) The  $^1\text{H}$  NMR spectra of different electrolytes. (d) Distribution of DME and TFSI $^-$  coordinated Mg ions in MD trajectories. (e) The DME ligand exchange rates of 0.5 M Mg(TFSI) $_2$ /DME and 0.5 M Mg(TFSI) $_2$  + 0.5 M MgBr $_2$ /DME electrolytes at 400 K obtained in the MD simulated trajectories.

(Fig. S14) shows that the dissolution of functional layer reduces the anodic stability of the electrolyte, which is similar with adding MgBr $_2$  to the electrolyte. The  $^1\text{H}$  NMR spectra of the blank electrolyte and modified electrolyte verified the dissolution of aniline magnesium bromide or its complexes in the electrolyte (Fig. S15).

The NMR peak of DME also has an interesting shift. As shown in Fig. 4c, the addition of Mg $^{2+}$  to DME makes peaks of DME shift to lower field, and the DME molecules encaging the Mg $^{2+}$  would form another two new peaks between 4.5–4.0 ppm [50,51]. After the addition of MgBr $_2$ , although the free DME peaks would not shift apparently, the encaging DME peaks almost disappears, implying the drastic changes in DME coordination. The same situation also occurs in the modified electrolyte, indicating that the dissolution of the functional layer has a great influence on the solvation structure in the electrolyte.

According to the previous EDS elemental analysis, the content of Br element in the sustained-release layer is much higher than that of N element, so the content of MgBr $_2$  should also be much higher than that of magnesium aniline bromide. Therefore, regarding the influence of the sustained-release layer on the solvation structure of electrolyte, we mainly discuss the effect of MgBr $_2$  dissolution on it. The molecular dynamic (MD) simulation is performed on 0.5 M Mg(TFSI) $_2$ /DME and 0.5 M Mg(TFSI) $_2$  + 0.5 M MgBr $_2$ /DME electrolytes and displayed in Fig. S16. The introduction of MgBr $_2$  in the electrolyte reduces the coordination number of DME and TFSI $^-$ . The more in-depth analysis of the simulated trajectory is carried out to acquire detailed information on distribution of the Mg $^{2+}$  solvation structure. As shown in the Fig. 4d, in the blank electrolyte, most of Mg $^{2+}$  are coordinated with three DME molecules. After the addition of MgBr $_2$ , the proportion of Mg $^{2+}$  with fully DME encaged decreases and is replaced by Br $^-$  or TFSI $^-$  coordinated species. With the dramatic transformation of Mg $^{2+}$  solvation structure distribution, inevitable change would occur in the activation energy during the Mg $^{2+}$  desolvation process. Therefore, the ligand exchange rates of electrolytes are calculated with the MD simulation to demonstrate a faster desolvation process in Br $^-$  containing electrolyte (Fig. 4e) [52]. In the Mg(TFSI) $_2$ /DME electrolyte, the exchange rate of

DME molecules with Mg $^{2+}$  ions is 1.14 ns $^{-1}$ , while that of Mg(TFSI) $_2$  + MgBr $_2$ /DME is enhanced to 6.0 ns $^{-1}$ , which indicates that coordination of Br $^-$  lead to the tremendous decline on the activation energy of Mg $^{2+}$  and account for the low plating overpotential of the modified Mg or modified electrolyte.

In brief, the functional layer of this work is a sustained-release layer of magnesium bromide/aniline magnesium bromide, which can be released and optimize Mg $^{2+}$  solvation structure after the addition of electrolyte. Compared to electrolyte modifications, the residual sustained-release layer maintains the freshness of SEI and reduces impedance of the SEI (Fig. S17), as well as the continuously released MgBr $_2$  and other components is more beneficial to compensate their consumption in the following cycles [47,53], resulting in a better electrochemical performance of the modified Mg electrodes.

#### 2.4. Interphases on cycled Mg

The interphases of cycled Mg electrodes are characterized to evaluate the passivation and Mg plating uniformity. With the bare Mg and blank electrolyte, the plated Mg appears as a large spherical shape with cracks (Fig. 5a and Fig. S18a), and the interphases of the Mg contains considerable C, O, F and S element (Table S3), which are generated from the decomposition of electrolyte. In comparison, after replacing the bare Mg with the modified Mg, the morphology of the plated Mg becomes smoother and firmer (Fig. 5b and Fig. S18b). Similar superiority in plated Mg morphology can also be detected from the SEM images of the bare Mg electrodes after cycled with modified electrolyte and MgBr $_2$  added electrolyte (Fig. 5c-d and Fig. S18c-d). However, it is difficult to distinguish the morphology of plated Mg in different modification strategies and explain the shorter lifespan of cells of the modified electrolyte and MgBr $_2$  additive. Therefore, the decomposed component produced by electrolyte decomposition in different conditions are characterized by EDS and XPS. The Table S3 and Fig. S19-22 shown the C, N, O, F and S element, which are related with anion and solvent decomposition, on bare Mg electrodes cycled in blank, modified

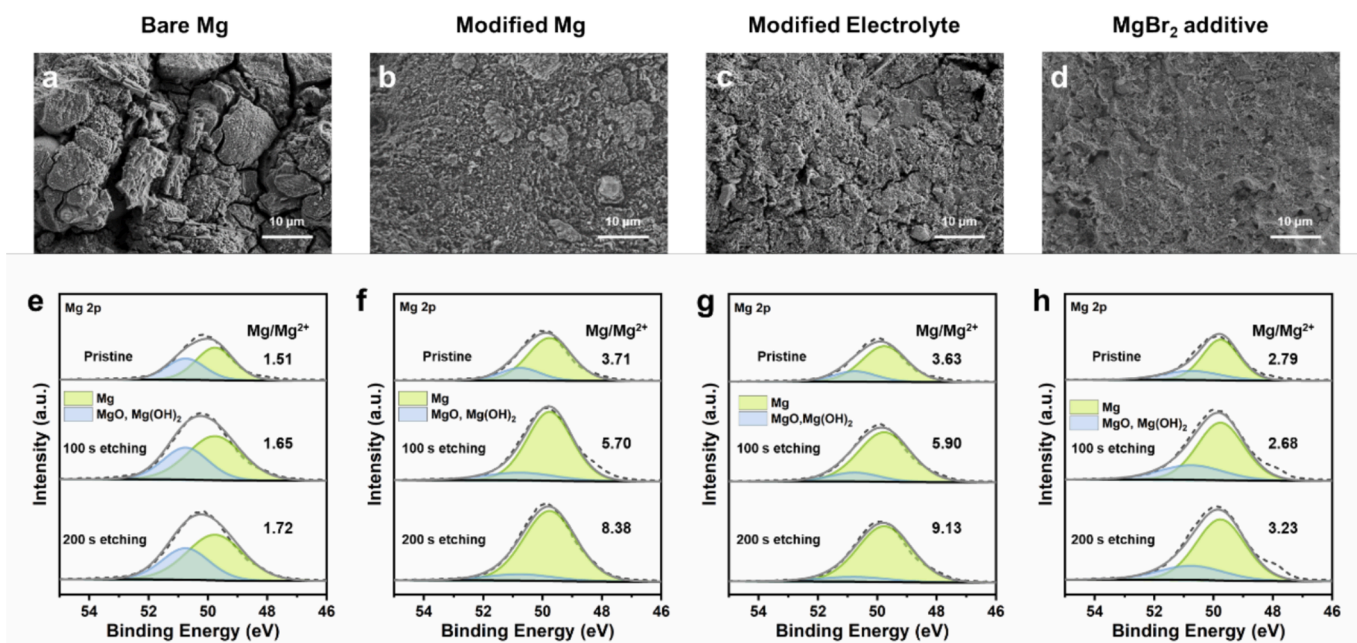


**Fig. 5.** The surface SEM images of the (a) bare Mg and (b) modified Mg electrodes after cycled with 0.5 M Mg(TFSI)<sub>2</sub>/DME electrolyte. The surface SEM images of the bare Mg electrodes after cycled with (c) modified electrolyte and (d) 0.5 M Mg(TFSI)<sub>2</sub> + 0.5 M MgBr<sub>2</sub>/DME. High-resolution XPS Mg2p spectra of the (e) bare Mg and (f) modified Mg electrodes after cycled with 0.5 M Mg(TFSI)<sub>2</sub>/DME electrolyte. High-resolution XPS Mg2p spectra of the bare Mg electrodes after cycled with (g) modified electrolyte and (h) 0.5 M Mg(TFSI)<sub>2</sub> + 0.5 M MgBr<sub>2</sub>/DME.

electrolyte, MgBr<sub>2</sub> added electrolyte are much higher than those on modified Mg. The XPS can show the relative content of various decomposition products more directly, as shown in Fig. 5e-h and Fig. S23-27. The order of the Mg/Mg<sup>2+</sup> ratio on cycled Mg is modified electrolyte > modified Mg > MgBr<sub>2</sub> additive > blank, verifying the higher Coulombic efficiency of modified Mg and modified electrolyte. The lower Mg/Mg<sup>2+</sup> ratio of modified Mg than the modified electrolyte can be explained by the remaining functional layer. The higher Coulombic efficiency of the modified Mg and modified electrolyte can be attributed to the aniline magnesium bromide and its polymers that can eliminates contaminants such as trace water in electrolyte and adsorbed on Mg to hinder the passivation of the anode/electrolyte interphase, which has more obvious advantages than the simple MgBr<sub>2</sub> additive.

### 2.5. Full battery demonstration

The Mg anode with this sustained-release layer are matched with CMK-3/S and Mo<sub>6</sub>S<sub>8</sub> cathodes respectively and compared with the battery of bare Mg anode to verify the compatibility between the modified Mg anode and cathode. As shown in Fig. 6a, the modified Mg dramatically reduces the overpotential and eliminates the voltage hysteresis of the Mg||CMK-3/S battery during discharge/charge process. For the Mg||Mo<sub>6</sub>S<sub>8</sub> battery, when the bare Mg is adopted as anode, battery has almost no capacity (Fig. 6b). By contrast, when the modified Mg is matched with Mo<sub>6</sub>S<sub>8</sub>, overpotential during discharge/charge is reduced to ~ 0.25 V (Fig. 6c). The Mg||Mo<sub>6</sub>S<sub>8</sub> battery with the modified Mg anode shows an initial specific capacity of 134.1 mAh/g and remains 68.6 mAh/g after 300 cycles at the current density of 25 mA g<sup>-1</sup> (Fig. 6d). Even at the higher current density of 100 mA g<sup>-1</sup>, as shown in Fig. S28, Mg||Mo<sub>6</sub>S<sub>8</sub> battery with the modified Mg anode reaches a high specific capacity of 66.2 mAh/g and a low overpotential below 0.35 V after 300 cycles. The performance of Mg||Mo<sub>6</sub>S<sub>8</sub> battery with the modified electrolyte and 0.5 M Mg(TFSI)<sub>2</sub> + 0.5 M MgBr<sub>2</sub>/DME are exhibited in Fig. S29-30. Both of their capacity and overpotential are between batteries with bare Mg and modified Mg, as well as the lifespan are shorter than batteries with modified Mg.

### 3. Conclusion

In summary, a functional layer with sustained-release effect is constructed on the Mg metal by ex-situ reaction between p-BAn and Mg. By XRD, ATR-IR and XPS characterization, it is proved that the functional layer contains a large amount of MgBr<sub>2</sub>, aniline magnesium bromide and their complexes. However, it has been demonstrated that MgBr<sub>2</sub> and aniline magnesium bromide on the Mg surface are partially dissolved in the electrolyte and improve electrochemical performance of Mg anode. The experiment and theoretical calculation certified that the dissolved MgBr<sub>2</sub> has a great influence on the Mg<sup>2+</sup> solvation structure distribution and accelerates the desolvation process dramatically. By comparison with various modification methods in terms of improving Coulombic efficiency and inhibition of side reactions, the Mg metal modification is still the best method compared with the modified electrolyte, which are attributed to the residual Br<sup>-</sup> after dissolution by electrolyte and the aniline magnesium bromide that can eliminates contaminants and adsorbed on Mg, maintaining the freshness of SEI from beginning to end. Therefore, Mg electrodes with this functional layer maintains a low polarization voltage of 0.2–0.4 V at a high current density of 1.0 mA cm<sup>-2</sup> above 1000 h without short circuit. The Mg||Mo<sub>6</sub>S<sub>8</sub> full battery presents a low overpotential of ~ 0.25 V during discharge/charge and remains 68.6 mAh/g after 300 cycles at the current density of 25 mA g<sup>-1</sup>. This work provides a new inspiration for developing high efficiency Mg metal anode and studying the mechanism of functional layer on Mg metal.

### CRedit authorship contribution statement

**Yichao Zhuang:** Writing – original draft, Visualization, Validation, Methodology, Investigation, Formal analysis, Data curation, Conceptualization. **Haiming Hua:** Writing – review & editing, Validation, Software, Methodology, Data curation. **Yaoqi Xu:** Writing – review & editing, Validation, Investigation. **Fei Wang:** Writing – review & editing, Validation. **Jiayue Wu:** Writing – review & editing, Validation. **Jing Zeng:** Writing – review & editing, Validation, Supervision, Project administration, Funding acquisition, Conceptualization. **Jinbao Zhao:**

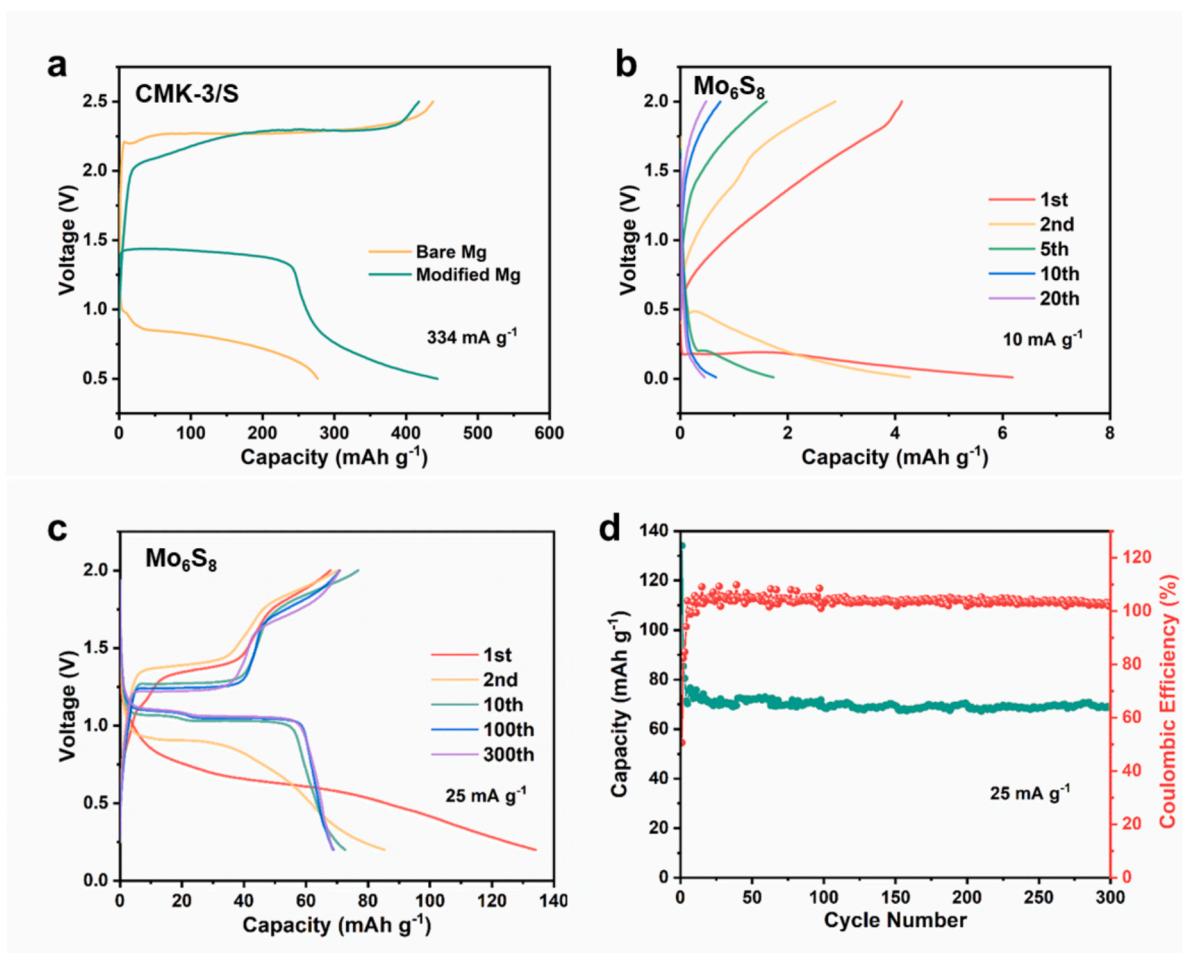


**Fig. 6.** (a) Discharge/charge profiles of Mg||CMK-3/S battery with bare Mg and modified Mg anode at the current density of 0.2C. Discharge/charge profiles of Mg||Mo<sub>6</sub>S<sub>8</sub> battery with 0.5 M Mg(TFSI)<sub>2</sub>/DME electrolyte and (b) bare Mg or (c) modified Mg anode at the current density of 25 mA g<sup>-1</sup>. (d) cycling performance of the modified Mg||Mo<sub>6</sub>S<sub>8</sub> batteries with 0.5 M Mg(TFSI)<sub>2</sub>/DME electrolyte at the current density of 25 mA g<sup>-1</sup>.

Writing – review & editing, Supervision, Resources, Project administration, Funding acquisition.

#### Declaration of competing interest

The authors declare that they have no known competing financial interests or personal relationships that could have appeared to influence the work reported in this paper.

#### Acknowledgment

The authors gratefully acknowledge the National Natural Science Foundation of China (No. 22005257), the Natural Science Foundation of Fujian Province of China (No. 2020 J05009) for financial support.

#### Appendix A. Supplementary data

Supplementary data to this article can be found online at <https://doi.org/10.1016/j.cej.2025.159445>.

#### Data availability

No data was used for the research described in the article.

#### References

- [1] J.B. Goodenough, K.-S. Park, The Li-ion rechargeable battery: a perspective, *J. Am. Chem. Soc.* 135 (2013) 1167–1176, <https://doi.org/10.1021/ja3091438>.
- [2] J.B. Goodenough, Y. Kim, Challenges for rechargeable Li batteries, *Chem. Mater.* 22 (2010) 587–603, <https://doi.org/10.1021/cm901452z>.
- [3] E. Fan, L. Li, Z. Wang, J. Lin, Y. Huang, Y. Yao, R. Chen, F. Wu, Sustainable recycling technology for Li-ion batteries and beyond: challenges and future prospects, *Chem. Rev.* 120 (2020) 7020–7063, <https://doi.org/10.1021/acs.chemrev.9b00535>.
- [4] R.C. Massé, E. Uchaker, G. Cao, Beyond Li-ion: electrode materials for sodium- and magnesium-ion batteries, *Sci. Ch. Mater.* 58 (2015) 715–766, <https://doi.org/10.1007/s40843-015-0084-8>.
- [5] J.W. Choi, D. Aurbach, Promise and reality of post-lithium-ion batteries with high energy densities, *Nat. Rev. Mater.* 1 (2016) 16013, <https://doi.org/10.1038/natrevmats.2016.13>.
- [6] F. Liu, T. Wang, X. Liu, L.Z. Fan, Challenges and recent progress on key materials for rechargeable magnesium batteries, *Adv. Energy Mater.* 11 (2020) 2000787, <https://doi.org/10.1002/aenm.202000787>.
- [7] C. You, X. Wu, X. Yuan, Y. Chen, L. Liu, Y. Zhu, L. Fu, Y. Wu, Y.-G. Guo, T. van Ree, Advances in rechargeable Mg batteries, *J. Mater. Chem. A* 8 (2020) 25601–25625, <https://doi.org/10.1039/d0ta09330k>.
- [8] H.D. Yoo, I. Shterenberg, Y. Gofar, G. Gershtinsky, N. Pour, D. Aurbach, Mg rechargeable batteries: an on-going challenge, *Energy Environ. Sci.* 6 (2013) 2265–2279, <https://doi.org/10.1039/c3ee40871j>.
- [9] C. Song, F. Shuang, L. Henan, S. Yumeng, Y. Hui Ying, Recent advances in kinetic optimizations of cathode materials for rechargeable magnesium batteries, *Coord. Chem. Rev.* 466 (2022) 214597, <https://doi.org/10.1016/j.ccr.2022.214597>.
- [10] R.E. Doe, R. Han, J. Hwang, A.J. Gmitter, I. Shterenberg, H.D. Yoo, N. Pour, D. Aurbach, Novel, electrolyte solutions comprising fully inorganic salts with high anodic stability for rechargeable magnesium batteries, *Chem. Commun.* 50 (2014) 243–245, <https://doi.org/10.1039/C3CC47896C>.
- [11] S.H. Lapidus, N.N. Rajput, X. Qu, K.W. Chapman, K.A. Persson, P.J. Chupas, Solvation structure and energetics of electrolytes for multivalent energy storage,

- Phys. Chem. Chem. Phys. 16 (2014) 21941–21945, <https://doi.org/10.1039/C4CP03015J>.
- [12] H. Singyuk, J. Xiao, G. Karen, W. Peng-fei, W. Luning, X. Jijian, S. Ruimin, B. Oleg, W. Chunsheng, Solvation sheath reorganization enables divalent metal batteries with fast interfacial charge transfer kinetics, *Science* 374 (2021) 172–178, <https://doi.org/10.1126/science.abg3954>.
- [13] A. Ran, S. Michael, H. Baruch, G. Yosef, A. Doron, Anode-electrolyte interfaces in secondary magnesium batteries, *Joule* 3 (2018) 27–52, <https://doi.org/10.1016/j.joule.2018.10.028>.
- [14] Z. Liang, C. Ban, Strategies to enable reversible magnesium electrochemistry: from electrolytes to artificial solid–electrolyte interphases, *Angew. Chem. Int. Ed.* 60 (2020) 11036–11047, <https://doi.org/10.1002/anie.202006472>.
- [15] D. Ramasubramanian, J.I. Brian, S.-Y. Reza, Progress in development of electrolytes for magnesium batteries, *Energy Storage Mater.* 21 (2019) 136–153, <https://doi.org/10.1016/j.ensm.2019.05.028>.
- [16] O. Mizrahi, N. Amir, E. Pollak, O. Chusid, V. Marks, H. Gottlieb, L. Larush, E. Zinigrad, D. Aurbach, Electrolyte solutions with a wide electrochemical window for rechargeable magnesium batteries, *J. Electrochem. Soc.* 155 (2008) A103–A109, <https://doi.org/10.1149/1.2806175>.
- [17] Y. Vestfried, O. Chusid, Y. Goffer, P. Aped, D. Aurbach, Structural analysis of electrolyte solutions comprising magnesium–aluminate chloro–organic complexes by raman spectroscopy, *organometallics* 26 (2007) 3130–3137, <https://doi.org/10.1021/om061076s>.
- [18] L.F. Wan, B.R. Perdue, C.A. Appleby, D. Prendergast, Mg desolvation and intercalation mechanism at the  $\text{Mo}_6\text{S}_8$  chevron phase surface, *Chem. Mater.* 27 (2015) 5932–5940, <https://doi.org/10.1021/acs.chemmater.5b01907>.
- [19] S. Chakrabarty, J.A. Blázquez, T. Sharabani, A. Maddegalla, O. Leonet, I. Urdampilleta, D. Sharon, M. Noked, A. Mukherjee, Stability of current collectors against corrosion in APC electrolyte for rechargeable Mg battery, *J. Electrochem. Soc.* 16 (2021) 080526, <https://doi.org/10.1149/1945-7111/ac1cc8>.
- [20] O. Tutusaus, R. Mohtadi, T.S. Arthur, F. Mizuno, E.G. Nelson, Y.V. Sevryugina, An efficient halogen-free electrolyte for use in rechargeable magnesium batteries, *Angew. Chem.* 127 (2015) 8011–8015, <https://doi.org/10.1002/ange.201412202>.
- [21] N.T. Hahn, T.J. Seguin, K.-C. Lau, C. Liao, B.J. Ingram, K.A. Persson, K.R. Zavadil, Enhanced stability of the carba-closio-dodecaborate anion for high voltage battery electrolytes through rational design, *J. Am. Chem. Soc.* 140 (2018) 11076–11084, <https://doi.org/10.1021/jacs.8b05967>.
- [22] S.-Y. Ha, Y.-W. Lee, S.W. Woo, B. Koo, J.-S. Kim, J. Cho, K.T. Lee, N.-S. Choi, Magnesium(II) bis(trifluoromethane sulfonyl) imide-based electrolytes with wide electrochemical windows for rechargeable magnesium batteries, *ACS Appl. Mater. Interfaces* 6 (2014) 4063–4073, <https://doi.org/10.1021/am405619v>.
- [23] E.N. Keyzer, H.F.J. Glass, Z. Liu, P.M. Bayley, S.E. Dutton, C.P. Grey, D.S. Wright,  $\text{Mg}(\text{PF}_6)_2$ -based electrolyte systems: understanding electrolyte–electrode interactions for the development of Mg-ion batteries, *J. Am. Chem. Soc.* 138 (2016) 8682–8685, <https://doi.org/10.1021/jacs.6b04319>.
- [24] I. Shterenberg, M. Salama, H.D. Yoo, Y. Gofar, J.-B. Park, Y.-K. Sun, D. Aurbach, Evaluation of  $(\text{CF}_3\text{SO}_2)_2\text{N}^-$  (TFSI) based electrolyte solutions for Mg batteries, *J. Electrochem. Soc.* 162 (2015) A7118–A7128, <https://doi.org/10.1149/2.0161513jes>.
- [25] N.N. Rajput, X. Qu, N. Sa, A.K. Burrell, K.A. Persson, The coupling between stability and ion pair formation in magnesium electrolytes from first-principles quantum mechanics and classical molecular dynamics, *J. Am. Chem. Soc.* 137 (2015) 3411–3420, <https://doi.org/10.1021/jacs.5b01004>.
- [26] T.J. Seguin, N.T. Hahn, K.R. Zavadil, K.A. Persson, Elucidating non-aqueous solvent stability and associated decomposition mechanisms for Mg energy storage applications from first-principles, *Front. Chem.* 7 (2019) 175, <https://doi.org/10.3389/fchem.2019.00175>.
- [27] F. Wang, H. Hua, D. Wu, J. Li, Y. Xu, X. Nie, Y. Zhuang, J. Zeng, J. Zhao, Solvent molecule design enables excellent charge transfer kinetics for a magnesium metal anode, *ACS Energy Lett.* 8 (2022) 780–789, <https://doi.org/10.1021/acsenergylett.2c02525>.
- [28] J. Zhang, J. Liu, M. Wang, Z. Zhang, Z. Zhou, X. Chen, A. Du, S. Dong, Z. Li, G. Cui, The origin of anode-electrolyte interfacial passivation in rechargeable Mg-metal batteries, *Energy Environ. Sci.* 16 (2023) 1111–1124, <https://doi.org/10.1039/d2ee03270h>.
- [29] S. Seoung-Bum, T. Gao, P.H. Steve, K.X. Steirer, S. Adam, N. Andrew, C. Wang, C. Arthur, K. Xu, C. Ban, An artificial interphase enables reversible magnesium chemistry in carbonate electrolytes, *Nature Chem.* 10 (2018) 532–539, <https://doi.org/10.1038/s41557-018-0019-6>.
- [30] B. Li, M. Robert, C. Liu, Y. Hu, W. Li, G. Zhang, G. Cao, Kinetic surface control for improved magnesium–electrolyte interfaces for magnesium ion batteries, *Energy Storage Mater.* 22 (2019) 96–104, <https://doi.org/10.1016/j.ensm.2019.06.035>.
- [31] Y. Li, P. Zuo, R. Li, H. Huo, Y. Ma, C. Du, Y. Gao, G. Yin, S.W. Robert, Formation of an artificial  $\text{Mg}^{2+}$ -permeable interphase on Mg anodes compatible with ether and carbonate electrolytes, *ACS Appl. Mater. Interfaces* 13 (2021) 24565–24574, <https://doi.org/10.1021/acsami.0c22520>.
- [32] Y. Zhang, J. Li, W. Zhao, H. Dou, X. Zhao, Y. Liu, B. Zhang, X. Yang, Defect-free metal–organic framework membrane for precise ion/solvent separation toward highly stable magnesium metal anode, *Adv. Mater.* 34 (2021) 2108114, <https://doi.org/10.1002/adma.202108114>.
- [33] H. Ye Yeong, L. Nam Kyeong, P. Sol Hui, S. Jisu, L., Yun Jung, TFSI anion grafted polymer as an ion-conducting protective layer on magnesium metal for rechargeable magnesium batteries, *Energy Storage Mater.* 51 (2022) 108–121, <https://doi.org/10.1016/j.ensm.2022.06.014>.
- [34] P. Clément, H. Arthur, L. Jean-Bernard, F. Dominique, A. Joachim, C. Jean-Noel, L. Olivera, B. Jan, D. Robert, D. Rémi, et al., Alloying electrode coatings toward better magnesium batteries, *J. Mater. Chem. A* 10 (2022) 12104–12113, <https://doi.org/10.1039/d2ta02083a>.
- [35] M. Toshihiko, W. Mariko, Oxygen – a fatal impurity for reversible magnesium deposition/dissolution, *J. Mater. Chem. A* 11 (2023) 9755–9761, <https://doi.org/10.1039/d3ta01286g>.
- [36] R. Lv, X. Guan, J. Zhang, Y. Xia, J. Luo, Enabling Mg metal anodes rechargeable in conventional electrolytes by fast ionic transport interphase, *Nat. Sci. Rev.* 7 (2019) 333–341, <https://doi.org/10.1093/nsr/nwz157>.
- [37] B. Wan, H. Dou, X. Zhao, J. Wang, W. Zhao, M. Guo, Y. Zhang, J. Li, Z. Ma, X. Yang, Three-dimensional magnesophilic scaffolds for reduced passivation toward high-rate Mg metal anodes in a noncorrosive electrolyte, *ACS Appl. Mater. Interfaces* 12 (2020) 28298–28305, <https://doi.org/10.1021/acsami.0c07213>.
- [38] Y. Zhao, A. Du, S. Dong, F. Jiang, Z. Guo, X. Ge, X. Qu, X. Zhou, G. Cui, A bismuth-based protective layer for magnesium metal anode in noncorrosive electrolytes, *ACS Energy Lett.* 6 (2021) 2594–2601, <https://doi.org/10.1021/acsenergylett.1c01243>.
- [39] Y. Li, X. Zhou, J. Hu, Y. Zheng, M. Huang, K. Guo, C. Li, Reversible Mg metal anode in conventional electrolyte enabled by durable heterogeneous SEI with low surface diffusion barrier, *Energy Storage Mater.* 46 (2021) 1–9, <https://doi.org/10.1016/j.ensm.2021.12.023>.
- [40] J. Bae, H. Park, X. Guo, X. Zhang, J.H. Warnera, G. Yu, High-performance magnesium metal batteries via switching the passivation film into a solid electrolyte interphase, *Energy Environ. Sci.* 14 (2021) 4391–4399, <https://doi.org/10.1039/d1ee00614b>.
- [41] R. Zhang, C. Cui, R. Li, Y. Li, C. Du, Y. Gao, H. Huo, Y. Ma, P. Zuo, G. Yin, An artificial interphase enables the use of  $\text{Mg}(\text{TFSI})_2$ -based electrolytes in magnesium metal batteries, *Chem. Eng. J.* 426 (2021) 130751, <https://doi.org/10.1016/j.cej.2021.130751>.
- [42] Y. Li, G. Yang, C. Zhang, W.Y. Lieu, C.Y.J. Lim, S. Sun, J. Wang, S. Jiang, Z. Xing, Z. Sofer, M. Ng, W. Liu, Z.W. She, Grain-boundary-rich triphasic artificial hybrid interphase toward practical magnesium metal anodes, *Adv. Funct. Mater.* 33 (2022) 2210639, <https://doi.org/10.1002/adfm.202210639>.
- [43] M. Hu, G. Li, K. Chen, X. Zhou, C. Li, A gradient structured SEI enabling record-high areal capacity anode for high-rate Mg metal batteries, *Chem. Eng. J.* 480 (2023) 148193, <https://doi.org/10.1016/j.cej.2023.148193>.
- [44] B. Yang, L. Xia, R. Li, G. Huang, S. Tan, Z. Wang, B. Qu, J. Wang, F. Pan, Superior plating/stripping performance through constructing an artificial interphase layer on metallic Mg anode, *J. Mater. Sci. Technol.* 157 (2023) 154–162, <https://doi.org/10.1016/j.jmst.2023.01.054>.
- [45] Y. Zhuang, D. Wu, F. Wang, Y. Xu, J. Zeng, J. Zhao, Tailoring a hybrid functional layer for Mg metal anodes in conventional electrolytes with a low overpotential, *ACS Appl. Mater. Interfaces* 14 (2022) 47605–47615, <https://doi.org/10.1021/acsaami.2c11911>.
- [46] A.R. Jeon, J. Seungyun, L. Gukhyun, J. Juyoung, N. Woo Joo, O. Si Hyoung, H. Jihyun, Y. Seung-Ho, L. Minah, Reversible magnesium metal cycling in additive-free simple salt electrolytes enabled by spontaneous chemical activation, *ACS Nano* 17 (2023) 8980–8991, <https://doi.org/10.1021/acsnano.2c08672>.
- [47] Y. Liu, W. Zhao, Z. Pan, Z. Fan, M. Zhang, X. Zhao, J. Chen, X. Yang, Interfacial engineering of magnesophilic coordination layer stabilizes Mg metal anode, *Angew. Chem. Int. Ed.* 62 (2023) e202302617, <https://doi.org/10.1002/anie.202302617>.
- [48] M. Wang, W. Sun, K. Zhang, Z. Zhang, A. Du, S. Dong, J. Zhang, J. Liu, X. Chen, Z. Zhou, et al., Synergy between the coordination and trace ionization of co-solvents enables reversible magnesium electroplating/stripping behavior, *Energy Environ. Sci.* 17 (2024) 630–641, <https://doi.org/10.1039/d3ee02450d>.
- [49] L. Ge, Z. Peng, W. Wang, F. Tan, X. Wang, B. Su, X. Qiao, P.K. Wong,  $\text{g-C}_3\text{N}_4/\text{MgO}$  nanosheets: light-independent, metal-poisoning-free catalysts for the activation of hydrogen peroxide to degrade organics, *J. Mater. Chem. A* 6 (2018) 16421–16429, <https://doi.org/10.1039/c8ta05488f>.
- [50] M. Salama, I. Shterenberg, H. Gizbar, N.N. Eliaz, M. Kosa, K. Keinan-Adamsky, M. Afri, L.J.W. Shimon, H.E. Gottlieb, D.T. Major, et al., Unique behavior of dimethoxyethane (DME)/ $\text{Mg}(\text{N}(\text{SO}_2\text{CF}_3)_2)_2$  solutions, *J. Phys. Chem. C* 120 (2016) 19586–19594, <https://doi.org/10.1021/acs.jpcc.6b07733>.
- [51] W. Zhao, Z. Pan, Y. Zhang, Y. Liu, H. Dou, Y. Shi, Z. Zuo, B. Zhang, J. Chen, X. Zhao, X. Yang, Tailoring coordination in conventional ether-based electrolytes for reversible magnesium metal anodes, *Angew. Chem. Int. Ed.* 61 (2022) e202205187, <https://doi.org/10.1002/anie.202205187>.
- [52] H. Hua, F. Wang, F. Wang, J. Wu, Y. Xu, Y. Zhuang, J. Zeng, J. Zhao, Machine learning molecular dynamics insight into high interface stability and fast kinetics of low-cost magnesium chloride amine electrolyte for rechargeable magnesium batteries, *Energy Storage Mater.* 70 (2024) 103470, <https://doi.org/10.1016/j.ensm.2024.103470>.
- [53] J.G. Connell, B. Genorio, P.P. Lopes, D. Strmcnik, V.R. Stamenkovic, N. M. Markovic, Tuning the reversibility of Mg anodes via controlled surface passivation by  $\text{H}_2\text{O}/\text{Cl}^-$  in organic electrolytes, *Chem. Mater.* 28 (2016) 8268–8277, <https://doi.org/10.1021/acs.chemmater.6b03227>.